Flow-induced channelization in a porous medium

A. Mahadevan[1] , A.V. Orpe[2] , A. Kudrolli[3] , L. Mahadevan[4]

[1] *Woods Hole Oceanographic Institution,*
[2] *National Chemical Laboratory, Pune,*
[3] *Department of Physics, Clark University,*
[4] *School of Engineering and Applied Sciences, Department of Physics, Harvard University*

PACS 81.05.Rm – Porous materials; granular materials
PACS 92.40.Gc – Erosion and sedimentation; sediment transport

Abstract – Flow through a saturated, granular, porous medium can lead to internal erosion, preferential flow enhancement and the formation of channels within the bulk of the medium. We examine this phenomenon using a combination of experimental observations, continuum theory and numerical simulations in a minimal setting. Our experiments are carried out by forcing water through a Hele-Shaw cell packed with bidisperse grains. When the local fluid flow-induced stress exceeds a critical threshold, the smaller grains are dislodged and transported, thus changing the porosity of the medium and thence the local hydraulic conductivity and the development of erosional channels. The erosion is ultimately arrested due to the drop in the mean pressure gradient, while most of the flow occurs through the channels. These observations are consistent with a simple theoretical model for channelization in terms of a macroscopic multiphase description of erosion. We model a dynamical porosity field that evolves along with the volume fraction of the mobile and immobile grains in response to fluid flow. Numerical solutions of the resulting initial boundary value problem yield results for the dynamics and morphology that are in qualitative agreement with our experiments. In addition to providing a basis for channelization in porous media, our study highlights how heterogeneity in porous media may arise from flow as a function of the erosion threshold, and thus potentially offers the ability to control channelization.

The dynamics of fluid flow through porous continua is relevant over many orders of magnitude in length scale with applications that range from large scale flow through fractured rock in aquifers and oil reservoirs to small scale flows in natural and artificially engineered systems [1, 2]. In all these cases, flows are characterized by large variations in hydraulic conductivity of the medium. This heterogeneity is usually ascribed to processes associated with the formation and consolidation of the porous medium via the agglomeration of grains (in geology) and cells (in biology). But heterogeneity and channelization may also arise due to selective erosion of material in non-cohesive porous media. Indeed, flow-induced erosion on the surface of porous substrates has been implicated in the formation of patterns on planetary [3, 4], littoral [5] and laboratory [6, 9] scales that involve both unconsolidated and consolidated media [7]. Dissolution and liquefaction can also arise from reactive instabilities as seen in melt migration [11, 12] and cave formation [13]. Here we explore the purely physical erosive instabilities occurring in the bulk of fluid saturated materials where they can lead to internal channelization via the dynamic coupling of flow and changes in hydraulic conductivity.

To show how this happens, we start by describing some experiments that demonstrate how erosion and channelization can occur in a saturated porous medium (See Movie1 in SI). The experiments were carried out in a fluid-saturated porous medium confined to a vertical quasi-two dimensional chamber based on a Hele-Shaw cell filled with bi-disperse mixture of glass beads as shown in Fig. 1A. The width between the walls of the apparatus is such that gravity is unimportant owing to the formation of arches between walls [14]. As our porous medium, we chose to fill 60% of the initial volume with large beads (diameter $d_1 = 4 \pm 0.1$ mm) and 24% small beads ($d_2 = 0.7 \pm 0.1$ mm). The width of the chamber, chosen to be $1.2 \times d_1$, enables visualization of the porosity pattern, and allows the larger beads to be rearranged locally without being transported by the flow, while the smaller beads can be dislodged and transported through the matrix of large beads. Since only

the smaller beads can be eroded, we scale the porosity by the maximum attainable absolute porosity, 0.4. Then, the scaled porosity (or liquid volume fraction), is denoted by $\phi_l \in [0, 1]$. To observe the evolution of the porosity induced by fluid flow, we use a back-lighting technique and an intensity-density calibration that allows us to obtain the volume fraction of liquid (void fraction) or porosity as a function of space and time at a grid resolution of $d_1 \times d_1$ (4×4 mm^2) in 2-dimensions (Fig. 1C).

We control the inlet flow rate Q, which is applied uniformly to the lower boundary of the experimental domain to provide a uniform specific discharge $q = Q/A$ over the cross-sectional area A. Since the sudden imposition of a large flow rate (and pressure gradient) can cause the entire medium to fluidize, we gradually ramp up the flow rate at the inlet from 500 to 2500 cm^3/min over 3 hours so that q increases from 0.65 and 3.27 cm/s. The increase in flow rate is carried out smoothly, as well as in steps of 0.13 cm/s over time intervals of 600 s to allow equilibration intermittently, but the behavior is qualitatively the same in both cases (Fig. 1D). The outlet at the upper boundary is maintained at atmospheric pressure. By measuring the pressure at the inlet, we can determine the average pressure gradient. It increases linearly with the flow rate for a constant porosity material. This confirms that the flow within the porous medium obeys Darcy's law even after channels are formed. With each increment in the flow rate, erosion occurs for a few minutes before stopping. The porous medium which is initially fairly uniform in porosity, becomes increasingly heterogeneous as the flow rate is increased, as erosion generates regions of enhanced porosity that connect to form channels with high conductivity (Fig. 1B,C). Eventually, the erosion patterns coarsen with time and just a few channels preferentially conduct most of the flow.

As the flow rate is gradually increased, the flow-induced stress, i.e. the magnitude of the local pressure gradient, can exceed the local threshold required to dislodge and mobilize particles. The microscopic physics of failure is complicated in general owing to the formation of fragments of varying sizes and shapes. However, for our simple bidisperse medium, the process is somewhat simpler since the dominant erosive process involves the dislodgment and movement of the smaller grains from the interstices between the larger grains. This leads to a local increase in the hydraulic conductivity and a readjustment of the flow. As the material erodes and porosity increases, the pressure gradient drops below the critical erosive stress threshold and erosion stops. For every increment in the flow rate, the pressure gradient is raised above the threshold and leads to further erosion; this increases the porosity and thus reduces the pressure gradient, which falls below the threshold so that erosion stops. Thus, for a given flow rate, the hydraulic conductivity evolves in space and time until it reaches a steady state that is a function the initial heterogeneity in the porosity of the medium. Although deposition can act to mitigate the erosion patterns by decreasing

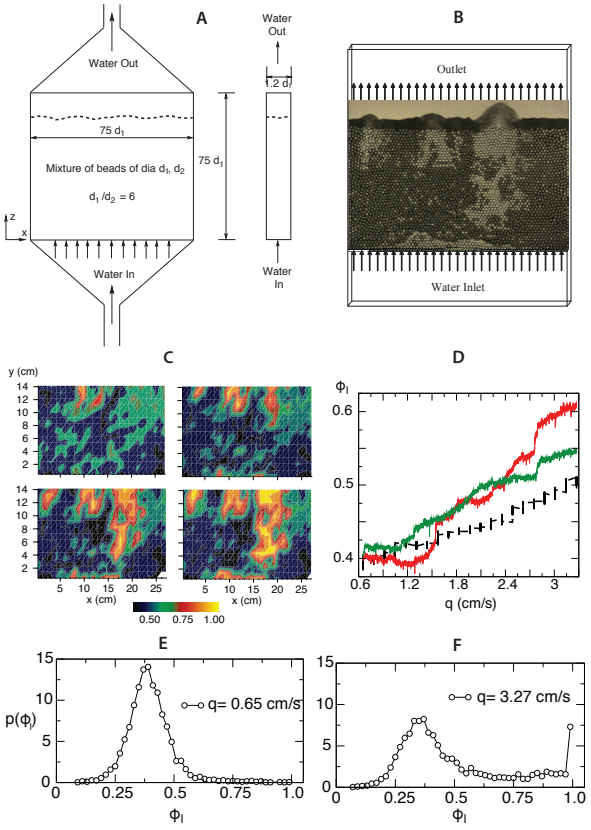

Fig. 1: Experiments – **A**: Schematic of the experimental set up showing face-on and sectional views. **B**: An instantaneous snap shot showing the spatially varying porosity generated by the flow. Light color indicates high porosity where the small beads have been removed by erosion. Small beads transported out of the porous medium are seen to pile up at the interface between the porous bed and clear water. **C**: Maps of the scaled porosity ϕ_l (absolute porosity normalized by the maximum attainable absolute porosity) for specific discharge rates q= 0.65, 1.3, 1.96 and 2.62 cm/s after the system has reached a steady state. **D**: Domain-averaged ϕ_l is plotted as a function of specific discharge q as it is ramped up over 3 hours (red and green curves) or stepped incrementally every 10 min intervals (black points) so as to achieve a near steady steady for each flow rate. Histogram or probability distribution of relative porosity $p(\phi_l)$ shown after steady state is achieved for a specific discharge rate **E:** $q = 0.65$cm/s and **F:**$q = 3.27$cm/s. For low discharge rates ($q = 0.65$cm/s in E), the peak in $p(\phi_l)$ is slightly broadened with respect to the initial condition but remains at the initialized value of $\phi_l = 0.4$. At higher discharge rates ($q = 3.27$cm/s in F) the distribution broadens further and a second peak that represents completely eroded channels is developed at $\phi_l = 1$.

the porosity and the hydraulic conductivity downstream, this effect is strongly dependent on whether the outflow region serves to sieve the mobile particles or trap them. The spatial pattern of porosity can vary significantly from one experiment to another due to the slight inhomogeneity in the initial conditions of the medium. However, in all cases, the basic phenomena is robust; preferential erosion, cou-

pled to conductivity and flow through positive feedback leads to the formation of channels of highly variable conductivity from a relatively uniform porous medium. The average porosity over the region is observed to increase linearly with flow rate for scaled porosity in the range 0.4–0.6 as shown in Fig. 1C,D. An example of the distribution (pdf) in porosity values over the region is shown in Figs. 1E,F for small and large flow rates, respectively. Initially, the distribution is broadly peaked at $\phi_l \sim 0.4$ corresponding to 60% large and 24% small beads. As the flow increases, a second peak develops at $\phi_l \sim 1$ corresponding to regions containing only large beads where complete erosion of the finer beads has occurred, a process that is concomitant with channelization.

Motivated by these qualitative observations, we now turn to a continuum theory for the dynamical evolution of channels via flow-induced erosion within a saturated porous medium. Our theory for the active co-evolution of the phases in a porous medium is qualitatively different from the single phase diffusive models for the evolution of free surfaces by aggregation and erosion [10] or multiphase bulk theories for multiple reactive fluids interacting with each other [11, 13] but yet combines features of both in considering the fluid-induced erosion and deposition processes acting in the bulk of a solid skeleton. To correctly account for the onset of erosion as well as its evolution as observed in the quasi-two dimensional bidisperse granular medium, we need to consider a multiphase theory that involves fluid, granular and immobile phases interacting with each other.

To enable a continuum field description of the process, we consider a representative volume much larger than the grain/pore size with $\phi_s(x, y, z, t)$ the volume fraction of the immobile solid phase, $\phi_g(x, y, z, t)$, the volume fraction of the granular mobile phase, and $\phi_l(x, y, z, t)$, the liquid volume fraction in the medium so that $\phi_s + \phi_g + \phi_l = 1$. We describe the time-evolution of these phases by accounting for the transport of the liquid and granular phases by velocities $\mathbf{u_l}$ and $\mathbf{u_g}$, respectively, and a transformation between phases by erosion and deposition. The erosion rate, e, is the rate of transformation of the immobile phase to mobile phase, d, is the rate of deposition or conversion of mobile phase to immobile phase. Volume conservation for the individual phases (each of which are assumed to be incompressible) implies that

$$\partial_t \phi_s = -e + d \quad (1)$$

$$\partial_t \phi_g = +e - d - \nabla \cdot (\phi_g \mathbf{u_g}) \quad (2)$$

$$\partial_t \phi_l = -\partial_t(\phi_s + \phi_g) = -\nabla \cdot (\phi_l \mathbf{u_l}) \quad (3)$$

We note that adding equations (1)-(3) yields the global continuity equation

$$\nabla \cdot (\phi_g \mathbf{u_g} + \phi_l \mathbf{u_l}) = 0. \quad (4)$$

For simplicity, we will assume that $\mathbf{u_g} = \mathbf{u_l} = \mathbf{u}$, i.e. the granular and liquid phases have the same velocity and the

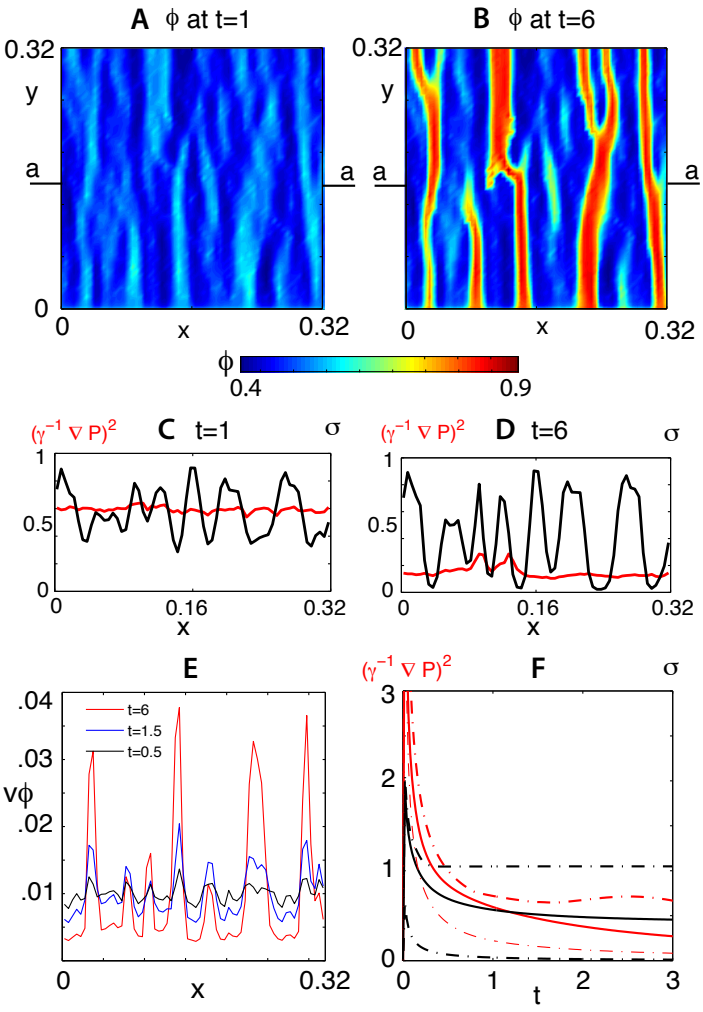

Fig. 2: Numerical solution to equations (1)–(7) with a steady specific discharge $q = q_0$ prescribed at the lower boundary $y = 0$, and constant pressure at the upper boundary $y = 0.32$. (A) Spatial distribution of porosity ϕ at $t = 1$ and (B) at t=6. (C) $(\gamma^{-1}\nabla P)^2$ (red) and σ (black) are plotted along a–a (at $y = 0.16$) at $t = 1$ and (D) at $t = 6$ corresponding to the panels above. Erosion occurs where $(\gamma^{-1}\nabla P)^2 > \sigma$. At early times, this occurs at several locations. As erosion progresses, the pressure gradient drops, heterogeneity in σ increases, and erosion is limited only to the channels. (E) The flux in the y-direction, $v(\phi_g + \phi_l)$ plotted at section a–a at $t = 0.5$ (black), $t = 1.5$ (red), and at $t = 6$ (blue). (F) As the flux increases in eroded regions, it decreases in non-channelized regions.

effects of inertia and body forces associated with sedimentation are negligible, a reasonable approximation for slow flows of nearly jammed grains. Then the continuity equation reduces to $\nabla \cdot \phi \mathbf{u} = 0$, where $\phi \equiv \phi_g + \phi_l$. To describe the rates of phase transformation e, from solid to mobile phase, and d, from mobile to solid phase. In a saturated porous medium, we postulate that erosion of ϕ_s can occur only when the fluid-induced stress exceeds a critical threshold σ. Then we may write the local convservation

rate from solid to granular phases as

$$e \quad = \quad k_e \phi_s \left((\gamma^{-1} \nabla p)^2 - \sigma \right) \geq 0, \tag{5}$$

where k_e is a characteristic rate and $\gamma = q_0/D_0$, the ratio of the characteristic specific discharge ($q_0 = 10^{-2} m/s$) to characteristic hydraulic conductivity ($D_0 = 10^{-6}$ m^{3}s kg^{-1}), is used to normalize the pressure gradient. The form of e follows from considerations of symmetry: a hydrostatic pressure p cannot lead to erosion, but a gradient can. However, the sign of the gradient is not important, so that we have chosen the simplest analytic dependence consistent with this symmetry (using the asymptotically correct but non-analytic form $|\nabla p|$ instead of $(\nabla p)^2$ yields qualitatively similar results - see Figure S1 in SI). The rate k_e is taken equal to the characteristic specific discharge q_0 divided by a characteristic length scale L; i.e. $k_e = q_0/L$ (where $q_0 = 0.01 m/s$ and $L = 1m$ as later described). The critical stress for erosion σ should be a function of the solid fraction ϕ_s. However, the non-local nature of elastic stress distribution in the porous medium warrants σ be more appropriately cast in terms of $\overline{\phi}_s = V^{-1} \int_V \phi_s dv$, a regional average of ϕ_s over a region V associated with a few grain volumes. This is because forces applied at a point decay over a length scale larger than the individual grain size. Although the form of σ is difficult to gauge from our experiments, we use the function $\sigma = 2(\tanh(2\pi(\overline{\phi}_s - 0.6)) + 1)$, where $0 \leq \overline{\phi}_s \leq 1$ which mimics the sharp dependence of the failure stress σ on the volume fraction

A simple model for d, the rate at which the mobile granular material is converted back to the immobile solid phase, is given by

$$d = k_d (\phi_s - \phi_s^*) \, \phi_g \geq 0. \tag{6}$$

The form of the deposition, with rate k_d, is based on a binary collision picture – mobile grains will come to rest only if they interact with immobile grains; hence the dependence on ϕ_s with a threshold ϕ_s^*. The rate k_d is taken as the characteristic specific discharge divided by a characteristic length scale; $k_d = q_0/L$.

In the porous medium, we assume that the volumetric flow rate per unit cross-sectional area, i.e. the specific discharge $\mathbf{q} \equiv \mathbf{u}(\phi_l + \phi_g)$, is given by Darcy's law[1]

$$\mathbf{q} \equiv \mathbf{u}\phi = -D(\phi) \nabla p, \text{ where } D = \frac{\phi^3 \, l_p^2}{A\mu \, (1 - \phi^2)}. \tag{7}$$

Here, $D(\phi)$, the hydraulic conductivity, is assumed to follow the Carman-Kozeny relation [2] and is in general a nonlinear function of the local fluid (pore) volume fraction $\phi = \phi_l + \phi_g$. Here l_p is the nominal pore size (which scales with the grain diameter), μ is the dynamic viscosity of the interstitial fluid, and the dimensionless constant $A = 180$ for spherical grains [2]. For $l_p = 1$mm, $\mu = 10^{-3}$ kg m^{-1}s^{-1}, D ranges from 0.6×10^{-7} – 1.6×10^{-5} m^{3}s kg^{-1} for ϕ between $0.1 - 0.9$.

[1]This can be generalized to a Brinkman-like equation if necessary in regions of high porosity.

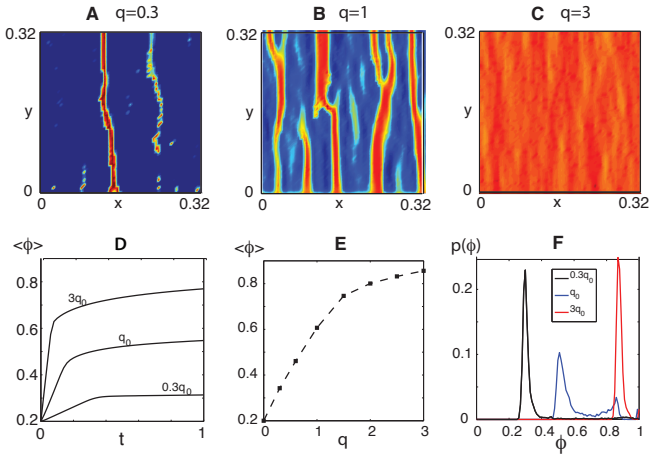

Fig. 3: The final distribution of porosity ϕ at $t = 6$ depending on the specific discharge q (scaled by q_0) specified at $y = 0$; (A) q=0.3, (B) q=1, (C) q=3. (D) For each q, the average porosity increases with time, until as steady state is achieved. (E) The final porosity (at $t = 6$) is a function of q at the inlet. (F) Histograms of the porosity distribution for $q = 0.3, 1$ and 3 shows bimodality and a peak at $\phi = 1$ due to channelization.

We use the domain size, $L = 1m$, specific discharge $q_0 = 1cm/s$, and time scale $T = L/q_0$ to make the problem dimensionless, so that the dimensionless parameters in the problem include the thresholds for erosion and deposition σ and ϕ_s^* as well as the ratio of deposition to erosion rates $\Pi_1 = \frac{k_d}{k_e}$, and the ratio of advection to erosion rate $\Pi_2 = \frac{q_0}{k_e L}$. Our choice of k_e and k_d implies that $\Pi_1 = \Pi_2 = 1$. We solve equations (1–7) numerically in 2-dimensions (x, y) using a finite volume method. In the x direction, we use periodic boundary conditions at $x = 0$ and $x = L_x$, with a square domain of dimension $L_x = 0.32, L_y = 0.32$ and a uniform grid resolution $\Delta = 0.05$. Prescribing the inlet pressure instead of the inlet discharge leads to either no erosion (if $(\gamma^{-1} \nabla p)^2 < \sigma$) or catastrophic erosion if the pressure gradients are larger than the threshold. Thus, we prescribe a constant scaled specific discharge $q_0 = 1$ at the inflow boundary $y = 0$, while at the outflow boundary $y = L_y$ we set pressure $p = 0$ (atmospheric pressure). The pressure is determined by iteratively solving the Poisson equation $\nabla(D(\phi)\nabla p) = 0$ obtained by substituting (7) into (4), then calculating the erosion rate e and the deposition rate d, and finally evolving equations (1)–(3) to update the volume fraction of the phases ϕ_s, ϕ_g, ϕ_l from one time step to the next, with time step $\Delta t = 10^{-4}$. Starting with an initial volume fraction of mobile grains $\phi_g = 0$ throughout the domain, and a mean liquid volume fraction $\phi_l = 0.2$ with an additive white Gaussian noise (standard deviation $sd = \sqrt{\langle \phi_l^2 \rangle - \langle \phi_l \rangle^2}^{1/2} = 0.01$) that leads to weak heterogeneity in σ, we allow the system to evolve until it reaches a quasi-steady state. The non-local form of the erosion threshold σ is based on $\overline{\phi}_s$, the weighted spatial average of ϕ_s, which is calculated

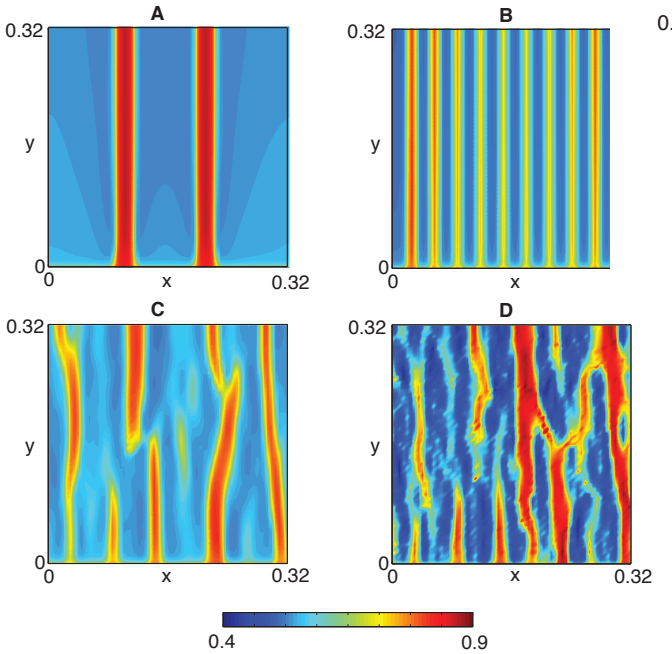

Fig. 4: The final distribution of porosity (at $t = 6$) is shown to be sensitive to the initial heterogeneity in σ arising from ϕ_s. The upper row shows the porosity distribution resulting when the initial distribution of ϕ_s is set to 0.8 everywhere, except in specific places where it is decreased by 1% from the uniform background value (A) along two lines, and (B) along 10 lines, each being one grid cell wide. In the lower row, the standard deviation (sd) in the initial perturbation to ϕ_s is varied from its previous value of $sd = 0.01$. (C) $sd = 0.001$. (D) $sd = 0.03$.

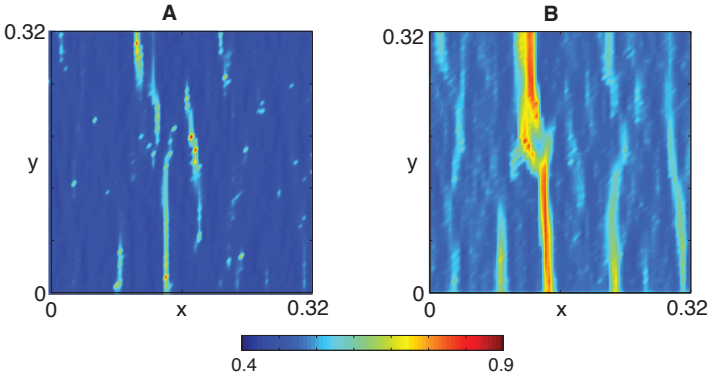

Fig. 5: The evolution of the porosity is sensitive to the functional form of the erosion threshold σ. Here the final distribution of porosity ϕ is shown for other choices of σ. (A) $\sigma = \overline{\phi}_s$, (B) $\sigma = \overline{\phi}_s^2$. These results can be compared with Fig. 1, where $\sigma = 0.5(\tanh(2\pi(\overline{\phi}_s - 0.6)) + 1)$ (subtracting 0.6 instead of 0.5 provides a slight asymmetry to the tanh profile.)

numerically as $\overline{\phi}_s(i,j) = 0.2\phi_s(i,j) + 0.1\phi_s(i \pm 1, j \pm 1)$. Averaging over the 8 surrounding neighbors of a grid point amounts to a radius of influence of the stress that extends a few grain diameters, in contrast to using a local value of ϕ_s that would lead to runaway erosion at individual grid cells.

In Fig. 2A,B we show two snapshots of the initially homogeneous porous medium as it erodes and channelizes (see Movie 2 in SI). This process involves positive feedback: flow is enhanced through the regions of low solid fraction (high hydraulic conductivity), while regions with a higher solid fraction and lower hydraulic conductivity are circumvented by the flow. Indeed, in Fig. 2C,D we see the interplay between the heterogeneity in the erosion threshold σ and the squared pressure gradient $(\gamma^{-1}\nabla p)^2$. The material is transformed from solid to mobile phase where $(\gamma^{-1}\nabla p)^2 > \sigma$ and transported by the flow, reducing $\overline{\phi}_s$, lowering σ, and augmenting erosion. The channelization leads to enhanced flow through regions of high hydraulic conductivity at the expense of low reduced flow through other regions (Fig. 2E) even as the total flow rate remains the same. In Fig. 2F, we provide a global view of the process. As erosion progresses, the average porosity and hydraulic conductivity over the entire domain increases. The pressure gradient required to sustain the same flow rate drops until it falls below the threshold for erosion almost everywhere and the system asymptotically approaches a steady state.

To understand how this steady state depends on the dimensionless parameters, we first vary the scaled specific discharge at the inlet q/q_0. When $q < q_c$, a critical scaled flow rate that depends on the initial porosity distribution in the medium, no erosion or channelization occurs, because the pressure gradient is everywhere smaller than the erosion threshold. For $q = q_c$, a single narrow channel and secondary partial channel are formed as shown in Fig. 3A. As q is increased further, the number of channels as well as the width of channels increases (Fig. 3B); for even higher flow rates, the entire medium begins to erode away as shown in Fig. 3C. In all cases, the porosity increases with time after initiation of the flow (Fig. 3D), linearly at first, and then slowly approaching a steady state value that depends on the inlet specific discharge. Much like the experiments, the average porosity of the medium is a function of the inflow q (Fig. 3E). Histograms of the porosity for varying inflow rates are shown in Fig. 3F; the case $q = 1$, produces the most bimodal porosity due to channelization.

Varying the erosion and deposition rates also leads to variations in the erosion patterns. In Fig. 4A we show the effect of a 10-fold increase in erosion rate k_e ($\Pi_1 = 0.1$), which leads to a faster evolution of channels. Increasing k_d 100-fold so that $\Pi_1 = 100$ increases the deposition rate and causes blockages that leads to termination and reinitiation of channels (Fig. 4B). In this model, deposition remains small even when $k_d = k_e$, because $\phi_g \ll \phi_l$ and a significant (100-fold) increase in k_d is needed before we begin to see the effects of deposition. The average number or size of channels does not change in either case relative to when $\Pi_1 = 1$ (corresponding to Fig. 2B).

A question that naturally arises is the mechanism for the selection of channel spacing and width when fluid flows

through a nominally homogeneous porous medium. The spacing and width of channels is insensitive to the domain size. Doubling the model domain size does not change the picture. The natural length scales in the problem are the system size L the nominal pore size l_p which evolves with time, but remains a microscopic length, and the length scales $q_0/k_e, q_0/k_d$; the latter control the dynamical evolution of the channels but not their final state. What remains is the threshold for erosion σ; since the onset of channelization is strongly influenced by fluctuations in the porosity (and thus the fragility) of the medium, we expect that linear stability analysis of the base state should predict that channels form at locations where σ is smallest initially. Thus for the same inlet specific discharge, the size and number of channels is a function of $\sigma(x, y, 0)$. In Fig. 4A we show that for a given inlet specific discharge, if $\sigma(x, y, 0) \equiv f(x)$ has a single minimum, a single channel forms and grows until the pressure gradient falls below the erosion threshold, while in Fig. 4B, we see that if $\sigma(x, y, 0)$ has multiple minima, multiple channels form. Of course, it is not sufficient to consider the mean value of the threshold; instead one must account for the complete probability distribution of the erosion threshold. For our simple Gaussian model of disorder, if the variance in the threshold for erosion (or equivalently the porosity fluctuations) is also changed, this leads to variations in the patterns as well. In Fig. 4C,D, we show that an increase in the standard deviation of the initial white noise leads to greater heterogeneity in the channel number and spacing.

Finally, we consider the functional form of the erosion threshold $\sigma(\overline{\phi}_s)$. In Fig. 5A we see that for $\sigma = \overline{\phi}_s$ the final morphology of the erosion patterns is more uniform compared to that shown in Fig. 5B for $\sigma = \overline{\phi}_s^2$, which is itself less variable than for the case when σ follows a $tanh$ profile (Fig. 1-4). We thus see that the form of the erosion threshold function, and its initial, possibly heterogeneous spatial distribution are crucial in determining the growth and form of the channels, which a simple linear analysis alone cannot capture.

Our model qualitatively captures the basic features of our physical experiments: below a critical flow rate, little or no erosion occurs. Above this threshold, the porous medium starts to erode heterogeneously at locations where the critical threshold is lowest; positive feedback then enhances erosion locally in other regions leading to oriented regions of higher porosity that are the hallmarks of channels. The modeled channels are not only able to branch, but also end and initiate, leaving dislocations in the medium. For a given flow rate, as channels form, the pressure gradient across the domain decays with time and the rate of erosion follows a similar trend in our numerical simulations. Consistent with this, we find an increase in the density of eroded channels and average porosity of the region for higher flow rates. In the experiments, the rate of erosion ceases abruptly when the pressure gradient falls below a threshold and small perturbations in the flow rate do not lead to further erosion. This is likely due to the effects of a nonlocal jamming process that does not have a counterpart in our theoretical description, where the erosion decays asymptotically for a constant flow rate. With increasing flow rates, our experiments show a linear increase in the average final porosity (Fig. 1D), a result that is mirrored in the numerical simulations (Fig. 3D) as well. The strong dependence of the channelization patterns on the heterogeneity of the initial porosity is, in addition, a feature of both our experiments and our numerical simulations. Indeed this is why we cannot predict the wavelength of the channelization patterns, which are instead determined by a combination of the prescribed flow rate and the initial distribution of variations in porosity.

Taken together, our qualitative experiments and continuum models allow us to move beyond the description of flow through porous media as just a passive response to its a priori prescribed hydraulic properties, and account for processes such as erosion, deposition, and dynamic permeability changes, to not only understand natural phenomena such as channelization, but also start to understand how one might control it in particular materials processing application.

* * *

We thank DOE NICCR (AM, AK), Harvard-NSF MRSEC (LM) and the MacArthur Foundation for partial support, and Andrew Fowler for comments on an earlier draft.

REFERENCES

[1] Scheidegger, A. E., 1960. The physics of flow through porous media. Macmillan Company, New York.
[2] Bear, J. 1972. Dynamics of fluids in porous media, Dover, New York, 1988.
[3] J. Harbor, B. Hallet, C. Raymond 1988. Nature, 333, 347-49.
[4] Malin, M. C. and Edgett, K., 2000. Science 288, 2330 - 2335.
[5] Hughes, Z.J., D.M. FitzGerald et al., 2009, Geophys. Res. Lett., 36, L03602.
[6] Schorghofer, N., Jensen, B., Kudrolli, A., and Rothman, D. H., 2004. J. Fluid Mech. 503, 357- 374.
[7] Cerasi, P. and Mills, P. 1998. Water Resources Res. 24, 1659- 1674.
[8] Jain, A.K. and Juanes, R. 2009. Phys. Rev. E 58(5), 6051-6060. J. Geophys. Res., 114 , B08101.
[9] Daerr, A., Lee, P., Lanuza, J., and Clement, E.. 2003. Phys. Rev. E 67, 06520.
[10] I. Rodriguez-Iturbe and A. Rinaldo, 1997. Fractal river basins. Cambridge University Press.
[11] D. McKenzie, 1984. J. Petrol., 25, 713.
[12] Spiegelman, M. 1993. J. Fluid Mech., 247:17-38.
[13] Szymczak, P. and Ladd, A.J. 2011 Geophysical Research Letters, 38: L07403.
[14] , Sperl, Matthias, 2006. Granular Matter, 8 *(2)*, 59-65.